



Mercury's magnetosphere

J.A. Slavin *

NASA GSFC, Laboratory for Extraterrestrial Physics, Code 696, Greenbelt, MD 20771, USA

Received 5 January 2003; received in revised form 27 February 2003; accepted 27 February 2003

Abstract

The Mariner 10 observations of Mercury's miniature magnetosphere collected during its close encounters in 1974 and 1975 are reviewed. Subsequent data analysis, re-interpretation and theoretical modeling, often influenced by new results obtained regarding the Earth's magnetosphere, have greatly expanded our impressions of the structure and dynamics of this small magnetosphere. Of special interest are the Earth-based telescopic images of this planet's tenuous atmosphere that show great variability on time scales of tens of hours to days. Our understanding of the implied close linkage between the sputtering of neutrals into the atmosphere due to solar wind and magnetospheric ions impacting the regolith and the resultant mass loading of the magnetosphere by heavy planetary ions is quite limited due to the dearth of experimental data. However, the influence of heavy ions of planetary origin (O^+ , Na^+ , K^+ , Ca^+ and others as yet undetected) on such basic magnetospheric processes as wave propagation, convection, and reconnection remain to be discovered by future missions. The electrodynamic aspects of the coupling between the solar wind, magnetosphere and planet are also very poorly known due to the limited nature of the measurements returned by Mariner 10 and our lack of experience with a magnetosphere that is rooted in a regolith as opposed to an ionosphere. The review concludes with a brief summary of major unsolved questions concerning this very small, yet potentially complex magnetosphere.

Published by Elsevier Ltd on behalf of COSPAR.

Keywords: Mercury's magnetosphere; Reconnection; Substorms

1. Introduction

Owing to its magnetic field, slow rotation rate, close proximity to the sun and lack of a dense atmosphere, Mercury occupies a unique position in the solar-planetary hierarchy (Russell et al., 1988). The magnitude of its magnetic moment is sufficiently large that it can stand-off the solar wind above the surface under most conditions, but it is weak to the point where Mercury occupies most of the forward magnetosphere. The volume threaded by magnetic flux tubes that are "closed" (i.e., both ends rooted in the planet) is so small that any "trapped" charged particle populations are expected to be transient and associated with recent substorm activity. However, the most significant difference between this magnetosphere and those of the other planets with global magnetic fields may be the tenuous nature of its atmosphere.

Planetary atmospheres are important sources of ions that may become assimilated into the magnetospheric charged particle populations. And, in turn, these atmospheres are major sinks for the energy drawn from the solar wind by their magnetospheres. At Mercury it appears that a unique situation exists where the magnetosphere couples directly to the regolith to create a source for new atmospheric neutrals through sputtering while simultaneously acting as a sink by sweeping up newly ionized atoms. Finally, the significance of Mercury's unique location deep in the inner heliosphere must be appreciated. Solar wind pressure and interplanetary magnetic field intensity at Mercury's perihelion are typically one order of magnitude higher than is the case at the Earth and more than two orders of magnitude greater than at Jupiter (e.g., see Slavin and Holzer, 1981).

Launched on November 2, 1973, Mariner 10 (M10) carried out an initial reconnaissance of the innermost planet during its three encounters with Mercury on March 29, 1974, September 21, 1974 and March 16, 1975. All fly-bys occurred at a heliocentric distance of

* Tel.: +1-301-286-5839; fax: +1-301-286-1648.

E-mail address: james.a.slavin@nasa.gov (J.A. Slavin).

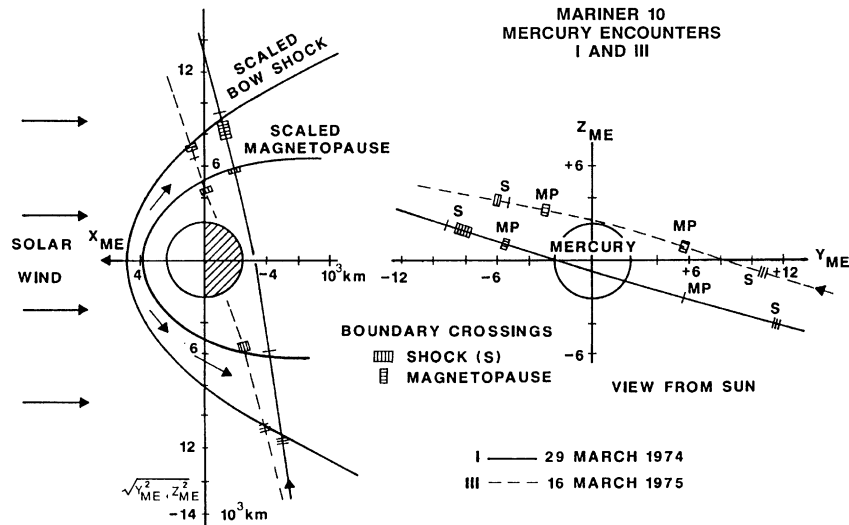


Fig. 1. The Mariner 10 trajectories during the first, MI, and third, MIII, encounters.

0.46 AU. This compares with perihelion and aphelion distances for this planet of 0.31 and 0.47 AU, respectively. The spacecraft trajectories during the first (MI) and third (MIII) encounters, which took it through Mercury's small magnetosphere, are displayed in Fig. 1 in Mercury centered solar ecliptic coordinates (from Ness et al., 1976). In these Mercury-ecliptic (ME) coordinates the X_{ME} axis is directed toward the sun and the Y_{ME} axis is in the plane of the ecliptic, perpendicular to X_{ME} and directed opposite to the direction of planetary orbital motion. The Z_{ME} axis completes the right-handed orthogonal system. The first encounter targeted the planetary "wake" in order to survey its interaction with the solar wind. The closest approach to the surface during this passage was 723 km and a peak magnetic field intensity of 98 nT was observed (Ness et al., 1974). The second encounter was directed well upstream of the planet to return images in full sunlight and did not contact the magnetosphere. The third encounter confirmed the global, dipolar nature of the magnetic field by sampling the magnetic field emanating from the polar regions where a maximum magnetic field of 400 nT was measured at the closest approach altitude of 327 km (Ness et al., 1976).

2. Magnetospheric structure

A schematic depiction of Mercury's magnetosphere based upon the Mariner 10 measurements is presented in Fig. 2. It has been drawn by taking an image of the Earth's magnetosphere and increasing the size of the planet by a factor of ~ 8 to compensate for the relative weakness of the dipole field and the high intensity of the solar wind pressure at 0.3–0.5 AU. This linear scaling was proposed by Ogilvie et al. (1977) and produces good

correspondence between the regional boundaries at the two planets. Hence, the mean $\sim 1.5R_M$ ($1R_M = 2439$ km) distance from the center of Mercury to the subsolar magnetopause found by M10 maps to about $12R_E$ ($1R_E = 6378$ km) at the Earth which is, indeed, near the average magnetopause nose distance. Similarly, the surface of Mercury would correspond to a distance just beyond geosynchronous orbit. For this reason the formation of a plasmasphere or trapped radiation belts, even if the planet possessed the sources and the rotation rate to create such a region (N.B., Mercury's rotational and orbital periods are 59 and 88 days, respectively) are not possible. Finally, the observed near-tail diameter of $\sim 5R_M$ scales to about $40R_E$ which is close to the mean diameter of Earth's tail.

During MI the magnetic field investigation observed clear bow shock and magnetopause boundaries along, with the lobes of the tail and the cross-tail current layer (Ness et al., 1974, 1975, 1976). Fig. 3 displays 1.2 s averages of magnetic fields measured during the first encounter in Mercury centered solar ecliptic coordinates. This encounter saw the spacecraft traverse the near-tail starting in the south lobe of the tail, crossing the inner edge of the current sheet, and eventually exiting through the dawn side magnetopause. Vertical dashed lines mark the inbound and outbound magnetopause boundaries as well as the point of closest approach (CA) to the planet. The tail-like nature of the magnetic field during the inbound passage is very evident with $|B_x| \gg |B_y|$ and $|B_z|$. The magnitude of the lobe magnetic field and the diameter of the tail provide a measure, via conservation of flux, of the co-latitude of the boundary of the "polar caps". These regions encompass the "open" magnetic field lines that connect the planet to the high latitude magnetosphere and the tail lobes before closing in the solar wind. The co-latitude of

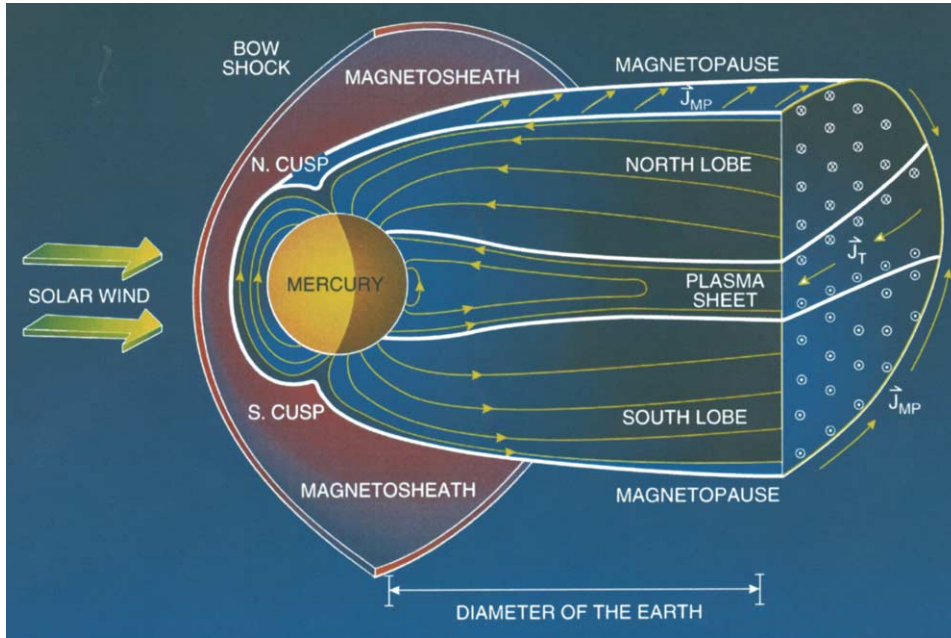


Fig. 2. Schematic view of the bow shock and magnetosphere of Mercury.

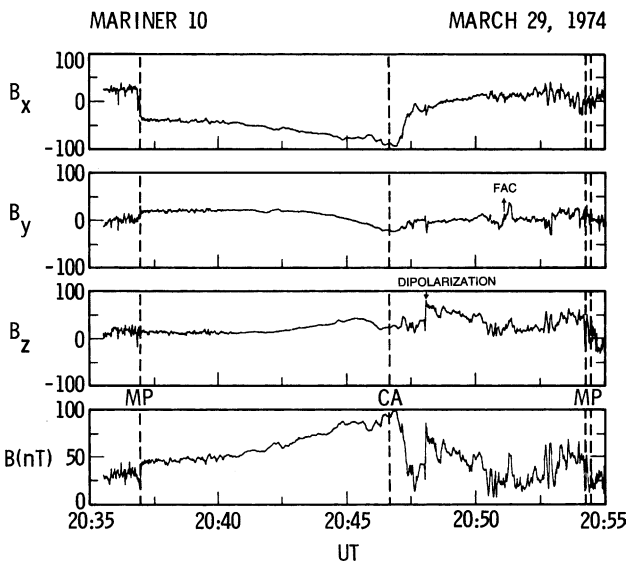


Fig. 3. The mariner 10 magnetic field observations (1.2 s average) taken during the first encounter.

the polar cap at Mercury is $\sim 25^\circ$ as compared with a value of $\sim 16^\circ$ at Earth indicating that the region of closed field lines are limited to lower latitudes than at the Earth. The existence of such a region of closed magnetic field lines is supported by the narrowband ~ 2 s period waves found by Russell (1989) in the MI magnetic field observations. These ULF waves are very similar to those frequently observed in the inner magnetosphere of the Earth suggesting that M10 did indeed penetrate into the closed field line region.

The magnetic field measurements taken during MIII encounter are displayed in Fig. 4 (from Ness et al., 1976). The interplanetary magnetic field (IMF) was directed northward both before and after the encounter. Hence, conditions were unfavorable for dayside reconnection and the input of energy into the magnetosphere and very smooth magnetic profiles were observed as shown in Fig. 4. The MII magnetic field measurements were of critical importance because they confirmed that the magnetosphere was indeed produced by the interaction of the solar wind with a global-scale magnetic field. Once corrected for the differing closest approach distances, the polar magnetic fields measured during MIII are about twice as large as those along the low latitude MI trajectory. This indicates that Mercury's magnetic field is primarily dipolar. Although significant uncertainties exist as to the contributions to the observed field by magnetospheric current systems and to higher order planetary magnetic fields, the magnitude of Mercury's dipole moment is between 300 and 500 nT $\cdot R_M^3$ with a tilt relative to the planetary rotation axis of about 10° (Connerney and Ness, 1988). Unfortunately, the spatial coverage provided by MI and MIII were not sufficient to separate out the contributions from higher order multipoles with any confidence (Connerney and Ness, 1988). Future progress will require not only a more spatially complete set of measurements, but also the development of more comprehensive and accurate magnetospheric current system models (Korth et al., 2004; Giampieri and Balogh, 2001).

The plasma investigation was hampered by a deployment failure which kept it from returning any ion

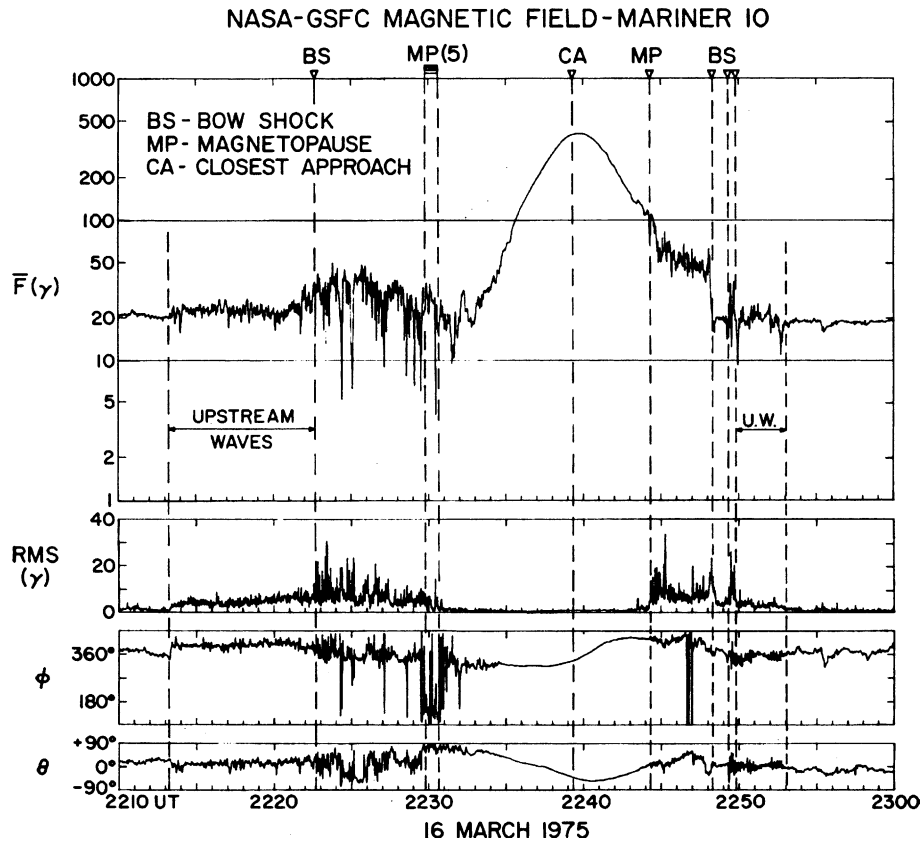


Fig. 4. Mariner 10 magnetic field observations made during the third fly-by on March 16, 1975.

measurements. Fortunately, the electron portion of the plasma instrument did work as planned (Ogilvie et al., 1974). For both passes good correspondence was found between the magnetic field and plasma measurements as to the locations of the bow shock and magnetopause boundaries. Furthermore, plasma speed and density parameters derived from the electron data produced consistent results regarding bow shock jump conditions and pressure balance across the magnetopause (Slavin and Holzer, 1979; Ogilvie et al., 1977). Within Mercury's magnetosphere, plasma density was found to be higher than that observed at Earth by a factor comparable to the ratio of the external solar wind density at the orbits of the two planets (Ogilvie et al., 1977). Throughout the MI pass plasma sheet-type distributions were observed with an increase in temperature beginning near closest approach coincident with the energetic particle events. In contrast, the MIII took the spacecraft through the high latitude magnetosphere where it observed the "horns" of a cool, quiet-time plasma sheet (Ogilvie et al., 1977; Ness et al., 1976).

3. Magnetospheric dynamics

The M10 observations have left the impression that Mercury's magnetosphere may be amongst the most

dynamic in the solar system. Whether or not this is true cannot be verified until more comprehensive, longer duration measurements are returned by the MESSENGER and BepiColombo, Missions (Solomon et al., 2001; Grard and Balogh, 2001). Following the same 8 to 1 scaling as used earlier, Fig. 5 displays some of the dynamic features that may be present at Mercury during magnetospheric substorm according to the near-earth neutral line (NENL) theory of substorms (Slavin et al., 2002; Baker et al., 1996). The reconnection x-line that typically forms ~ -20 to $-30R_E$ behind the Earth would be expected to lie at about $-3R_M$ at Mercury. This near-Mercury neutral line (NMNL) is the site where lobe magnetic field energy is dissipated to power high-speed plasma flow, plasma heating, and energetic particle acceleration. As shown in Fig. 5, "jets" of plasma emanate from the x-line with speeds comparable to the Alfvén speed in the flux tubes undergoing reconnection. These flows are usually very time dependent with the sunward and anti-sunward flows in the terrestrial magnetosphere being termed "bursty bulk flows" (Angelopoulos et al., 1992) and "post-plasmoid plasma sheet flows" (Richardson et al., 1987), respectively. The anti-sunward flows slow as they compress the dipolar magnetic fields closer to the planet and create a high pressure region that is thought to drive strong field-aligned currents into and out of the ionosphere called the "substorm current

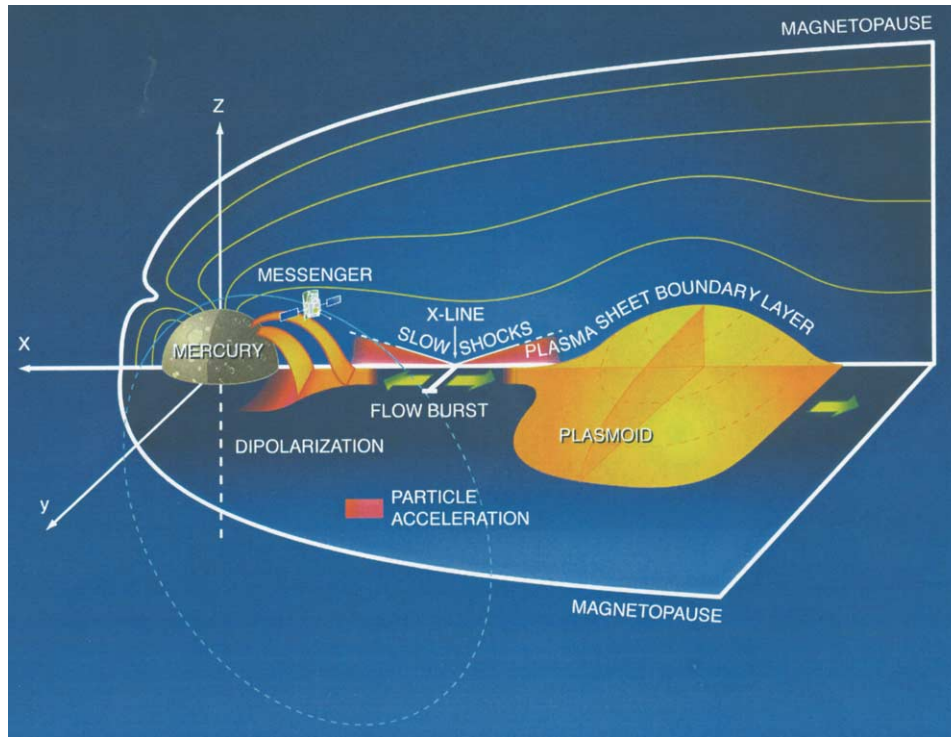


Fig. 5. A schematic view of the substorm expansion phase at Mercury based upon the NENL model.

wedge”, or SCW (Shiokawa et al., 1998). This slowing is most pronounced in the Earth’s magnetosphere at downtail distances of $X \sim -16$ to $-12R_E$ (Baumjohann et al., 1990) which should correspond to -2 to $-1.5R_M$ at Mercury. These high-speed flows often contain magnetic flux ropes or loop-like structures that have dimensions of a few Earth radii in the near-tail, but grow to have diameters of $\sim 10R_E$ or more in the distant downstream tail (Slavin et al., 1999; Ieda et al., 1998). An example of such a large tailward moving structure, called a plasmoid or plasmoid-type flux rope, in Mercury’s tail is depicted in Fig. 5 (in yellow). By the standard scaling rule, these plasmoids would be expected to grow to several Mercury radii in diameter.

Turning to the dayside interaction, the mean distance from the center of Mercury to the subsolar magnetopause based upon the M10 observations is about $1.5R_M$ (Russell, 1977; Ness et al., 1976). Slavin and Holzer (1979) further found that the subsolar distances extrapolated from the individual magnetopause and bow shock crossings, after scaling for upstream ram pressure effects, varied from 1.3 to $2.1R_M$ with the larger values corresponding to IMF $B_z > 0$ and the smaller to $B_z < 0$. They attributed this variability to the transfer, or “erosion”, of magnetic flux from the dayside magnetosphere into the tail. Whether or not the solar wind is ever able to compress and/or erode the dayside magnetosphere to the point where solar wind ions could directly impact the surface at low latitudes remains a topic of considerable

interest and controversy. Siscoe and Christoper (1975) were the first to take a long time series of solar wind ram pressure data taken at 1 AU, scale it by $1/r^2$ inward to Mercury’s perihelion, and then compute the solar wind stand-off distance using various assumed planetary magnetic moments. They found that only a few percent of the time will the magnetopause be expected to fall below an altitude of $\sim 0.1R_M$ or the point where solar wind protons will begin to strike the surface due to finite gyro-radius effects. Shorter lived, large amplitude increases in solar wind ram pressure associated with high-speed streams and interplanetary shocks might be expected to easily depress the magnetopause close to the surface of planet. However, theoretical models have shown that induction currents should be readily generated in the planetary interior to resist such rapid compressions (Glassmeier, 2000; Hood and Schubert, 1979). Moreover, model calculations by Suess and Goldstein (1979) have indicated that the magnetic flux added to the dayside magnetosphere by these induction currents becomes especially important as the magnetopause is compressed below $\sim 0.2R_M$. In fact, their model predicts that the ram pressure increase required to drive the magnetopause to $0.1R_M$ may be an order of magnitude more than what would be required in the absence of induction effects.

Magnetopause erosion is a well-known consequence of magnetic reconnection between the IMF and planetary magnetic fields and reduces the distance to the

subsolar magnetopause at the Earth by $\sim 1-2R_E$ for a typical interval of southward IMF (Sibeck et al., 1991). The most direct evidence that reconnection operates at Mercury's magnetopause takes the form of "flux transfer events" identified in the M10 data by Russell and Walker (1985). These discrete, flux rope-like structures are a well accepted signature of reconnection at the terrestrial magnetopause. Approximately $\sim 10-20\%$ of the southward IMF impinging upon the dayside magnetopause at the Earth undergoes this reconnection (see Slavin and Holzer, 1979) and is pulled back into the magnetotail. In the terrestrial magnetosphere excess magnetic flux in tail may be stored for tens of minutes to a few hours before rapid reconnection in the cross-tail current layer returns it to the dayside. The possibility exists that Mercury may lack the ability to store excess magnetic flux in its tail due to the effective absence of an electrically conducting ionosphere. Luhmann et al. (1998) have suggested, for example, that flux addition to the tail will rapidly lead to the reconnection of a like amount of flux in the tail. This would eliminate the "growth phase" of terrestrial substorms during which energy is stored in the tail prior to expansion phase onset (McPherron et al., 1973). However, even assuming Luhmann's hypothesis is correct, there would still be some minimal convection time delays in the magnetosheath and then the tail as the magnetic flux is transported to and from the dayside magnetosphere. Such a minimum convective "response time" was estimated by Slavin and Holzer to be ~ 2 min. The relationship between the inward displacements of the magnetopause at Mercury as a function of the magnetospheric response time, T_{rm} , scaled from average Earth observations is displayed in Fig. 6 (from Slavin and Holzer, 1979). On the basis of this analysis they proposed that the subsolar regions of the surface at Mercury may frequently be exposed to direct solar wind impact even if the magnetospheric response time is as short as 5 min. Finally,

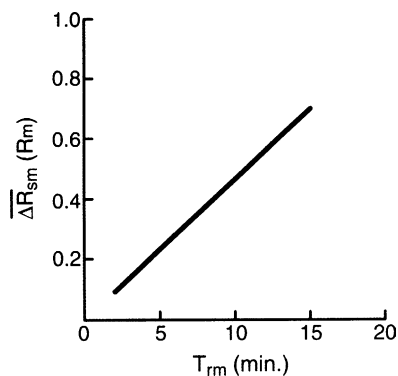


Fig. 6. Inward displacement of the subsolar magnetopause at Mercury as a function of the magnetospheric response time, T_{rm} , scaled from earth observations. Reproduced by permission of the American Geophysical Union.

these estimates of the effects of erosion on the shielding of the regolith provided by the dayside magnetosphere may be quite conservative because they do not take into account the increased efficiency of reconnection at Mercury due to the high Alfvén speeds in the solar wind at 0.3–0.5 AU.

Another potentially important aspect of the dayside magnetosphere dynamics at Mercury concerns the origins of the planet's very tenuous, collisionless neutral atmosphere, especially the three species (i.e., Na, K, and Ca) that can be measured spectroscopically from the Earth (Potter and Morgan, 1985, 1986). The large day-to-day variability in the sodium and potassium clouds at Mercury, including both changes in total density and its global distribution, can be quite striking in their telescopic images and may be linked to dynamic events in the solar wind and their effect on the magnetosphere. In particular, Potter et al. (1999) suggested that the underlying cause of large the day-to-day changes in the neutral clouds might be the modulation of the surface sputtering rates due to variations in the spatial distribution and intensity of solar wind proton impingement on the surface. Sarantos et al. (2001) investigated this hypothesis by taking a well tested terrestrial magnetospheric model, scaling it to Mercury, and examining the access of solar wind ions to the surface along magnetically open field lines. In doing so, they increased the efficiency of the reconnection process by 40% due to the high Alfvén speeds in the solar wind at 0.3 AU as suggested by Slavin and Holzer (1979). Fig. 7 (from Sarantos et al., 2001) shows an example of their results for $B_x = -40$ nT, $B_y = -5$ nT, and $B_z = -20$ nT. Pro-

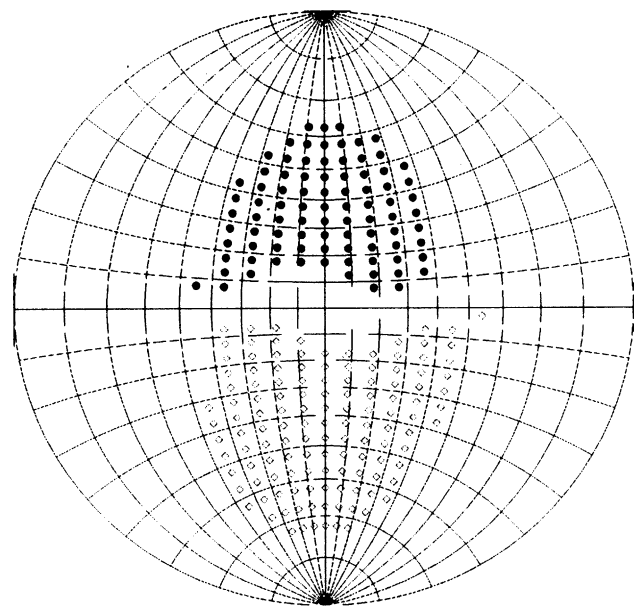


Fig. 7. Regions of open magnetic field that map to the upstream (black dots) and downstream (open diamonds) IMF.

jected down upon the dayside hemisphere are the foot prints of recently “opened” field lines that connect the planetary surface to the solar wind. The empty region at low latitudes corresponds to the small portion of the surface still shielded from the solar wind by closed magnetic field lines. The new feature uncovered is the strong asymmetry introduced by the very strong IMF B_x field component which results in the field lines emanating from the northern/southern hemispheres mapping to the upstream/downstream solar wind for negative/positive IMF B_x , respectively. Hence, the black dots and open diamonds in Fig. 7 both correspond to newly opened field lines, but only the northern hemisphere (i.e., black dots) connects to the upstream solar wind (for strongly negative B_x) and channels solar wind protons to the surface where sputtering may produce an enhanced outward flux of neutral atoms. Interplanetary sector crossings, for example, are a common source of reversals in the polarity of IMF B_x and could contribute to the neutral atmospheric variability observed by Potter et al. (1999) over Mercury’s poles by means of the hemispheric asymmetries predict by Sarantos et al. (2001).

Recently, a similar analysis has been carried out by Leblanc et al. (2003) for solar energetic particles (i.e., ions with energies >10 keV/amu) accelerated in association with coronal mass ejections. They also found that charged particle access to the surface of Mercury depended critically upon the IMF and that the fluxes of sputtered neutrals resulting from such surface impacts could be highly asymmetric and represent a possible explanation for Potter et al.’s variable neutral cloud distribution.

Many of the features found in the analytical models of Mercury’s magnetosphere are reproduced in the new global MHD and hybrid simulations of the solar wind interaction with this planet (Kallio and Janhunen, 2003; Ip and Kopp, 2002; Kabin et al., 2000). For example, as shown in Fig. 8 (from Kabin et al., 2000), the region of closed magnetic fields extended no farther poleward than $\sim 50^\circ$ latitude in good agreement with the analytical models. The magnetic fields emanating from the polar regions do indeed map back into the lobes of the tail, but with the strong north/north asymmetry in the draping of the newly opened flux tubes that was also found by Sarantos et al. (2001). In Fig. 8 the recently opened blue field lines that connect to the upstream solar wind and allow direct impact of solar wind ions on the surface while the white field lines only map to the downstream solar wind. Global MHD simulations by Ip and Kopp (2002) and hybrid simulations by Kallio and Janhunen (2002) produced qualitatively similar results, especially respect to the strong effects of IMF B_z and B_x on the magnetic topology of the dayside magnetosphere and its affect on interplanetary charged particle access to the surface.

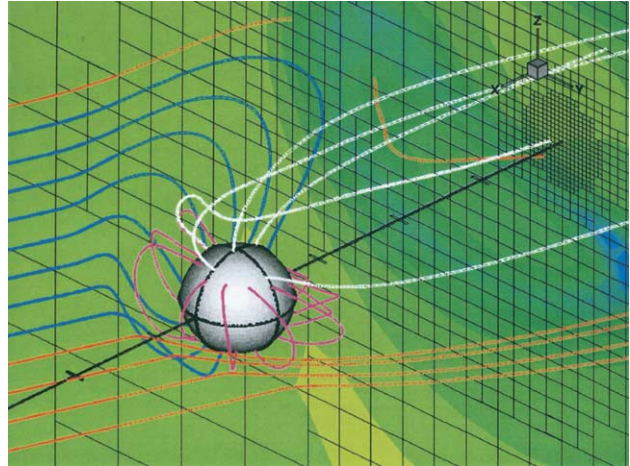


Fig. 8. MHD simulation of the magnetosphere of Mercury revealing flux tube topology via color coding; tan field lines are interplanetary, magenta field lines are closed, and white and blue field lines are open.

A substorm is a magnetosphere-wide disturbance that channels large amounts of electromagnetic energy, either drawn directly from the solar wind or first stored in the tail lobes, into plasma sheet heating, high speed bulk plasma flows, energetic particle acceleration, and field-aligned currents. In addition to producing large scale reconfiguration of the tail magnetic fields and high speed plasma flow, the magnetic and electric field changes during substorms act together to “inject” energetic particles into the inner magnetosphere where they drift about the Earth until lost due to charge exchange, scattering into the loss cone, or “shadowing” of the drift path by the magnetopause. Furthermore, the rapid B-field changes at x-lines produce large inductive electric fields that populate the “separatrix layers” between the x-line and the slow shocks that mark the outermost reconnected field lines with accelerated particles (Cowley, 1980). Observationally, spacecraft often observe energetic ions and electrons with energies of tens of keV to several MeV in the deep tail during substorms (Richardson et al., 1996; Sarris and Axford, 1979). On the sunward side of the x-line these charged particles will be further energized as they convected toward the planet and conserve their first adiabatic invariant. Hence, a particle transported from the Earth’s central plasma sheet to the ring current region could experience a factor of 10^3 or 10^4 increase in energy as the magnetic field intensity grows by a similar amount. At Mercury, by comparison, this type of “betatron” acceleration may raise the energy of the “seed” particles by only a factor of $\sim 10^2$ due to the relative weakness of the magnetic fields external to the planet.

As reported by Simpson et al. (1974), four separate, several minute long enhancements were recorded which they termed the A, B (and B’), C and D events. The nature of the particles being measured has been the

subject of some controversy because of instrumental effects associated with the extremely high count rates (Eraker and Simpson, 1986). However, the most likely source would appear to be electrons with energies greater than 35 keV (Christon, 1987). Each of the events is characterized by rapid rises followed by several minute long decays back to the background levels; albeit this behavior is least well defined for the relatively weak “A” event. All of the energetic particle events observed by M10 occurred during the outbound leg of MI when very disturbed magnetic fields were observed. Finally, it should be noted that the C event straddled the outbound magnetopause crossing while the D event was observed in the dawn side magnetosheath.

Detailed energetic particle and magnetic field measurements during the B–B’ event are provided in Fig. 9 (from Christon, 1987). Less than a minute after M10 entered the plasma sheet, i.e. the strong dip in magnetic field intensity beginning around 20:47 UT (see Fig. 3), there is a rapid increase in the B_z field component. As displayed in Fig. 9, the initial sudden B_z increase and subsequent quasi-periodic increases are nearly coincident with the enhancements in the flux of >35 keV electrons observed by the cosmic ray telescopes (Christon, 1987; Eraker and Simpson, 1986; Simpson et al.,

1974). This energetic particle event and several weaker ones observed later in the outbound pass were interpreted as evidence for substorm activity by both the original M10 investigators and subsequent studies (Eraker and Simpson, 1986; Baker et al., 1986; Siscoe et al., 1975). The Christon (1987) analysis of both the magnetic field and energetic particle signatures for this interval showed strong similarities to substorm injections commonly observed at the Earth. Similarly, the magnetic field signature in Fig. 9 is also seen frequently at the Earth and termed a “magnetic field dipolarization”. Such dipolarization events are closely associated with energetic particle injections and field-aligned currents. Investigations of the underlying physical processes causing these phenomena are still at the cutting edge of magnetospheric physics today.

Baker et al. (1986) and Christon (1987) suggested that each of the energetic particle events, A–D, observed, during the first M10 encounter was due to an individual substorm and the formation of a near-Mercury x-line in the tail. The subsequent injection of energetic electrons into the dipolar magnetic fields of the inner type magnetosphere and their eastward drift is diagrammed in Fig. 10 (from Baker et al., 1986). They estimated that the drift time is ~ 6 – 8 s for ~ 300 keV electrons assuming

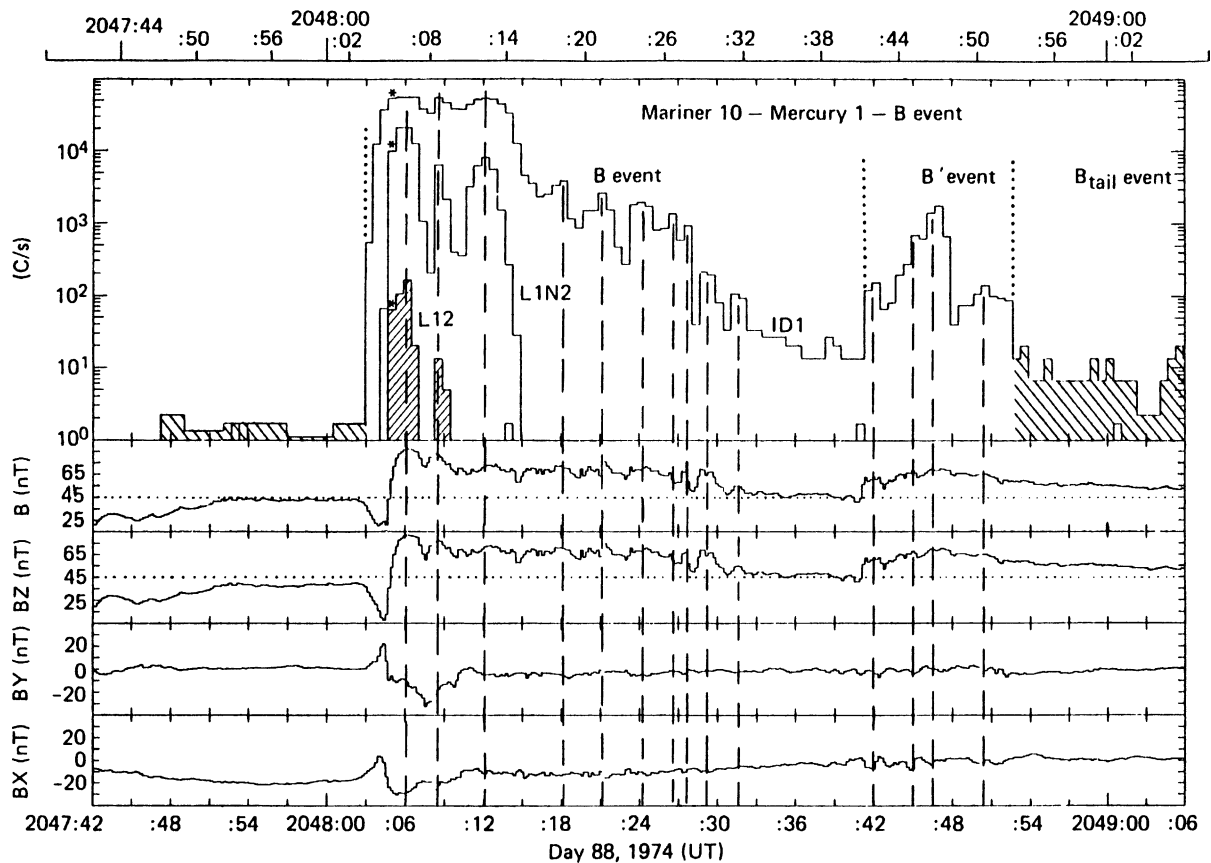


Fig. 9. Mariner 10 high time resolution (0.6 s) energetic electron (>35 keV) count rate (c/s) and magnetic field (0.04 s) measurements with vertical dashed lines marking increases in larger energetic particle event.

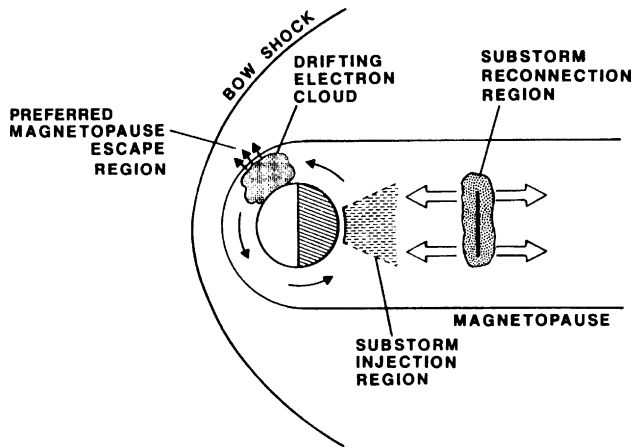


Fig. 10. Schematic view of energetic particle acceleration at a near-Mercury neutral line and subsequent “injection” into the inner magnetosphere. Reproduced by permission of the American Geophysical Union.

a closed path. The C and D events at the dawn magnetopause and in the magnetosheath were attributed to electrons being injected onto drift paths intersecting the dawn-side magnetopause. No energetic particle events were detected during the MIII high latitude encounter (Eraker and Simpson, 1986) presumably due to the northward IMF and lack of substorm activity at the time of that encounter.

Although not measured by M10, the drift trajectories for energetic ions in Mercury’s small magnetosphere have been the subject of extensive modeling. In particular, Lukyanov et al. (2001) investigated the fate of energetic protons originating in a $1R_M$ wide source region at the anticipated distance of the near-Mercury neutral line, $\sim 2\text{--}3R_M$ downstream of the planet. For energies ≤ 10 keV the ExB drift dominates the gradient and curvature drifts and the protons intercept the surface of Mercury near midnight. As the energy increases to 30–50 keV, the curvature and gradient drifts become more important and a partial ring forms about the planet with many ions hitting the planet on the dayside or escaping through the dawn-side magnetopause. Above 50 keV nearly all of the protons encounter the planetary surface or the magnetopause within a few seconds.

4. Electrodynamic coupling

Magnetospheres are tightly coupled to their planets by field-aligned currents (FACs) that flow along the magnetic lines of force linking the two. Any stress exerted upon the planetary magnetic field by the external solar wind or internal dynamics, such as reconnection and convection, generates field aligned currents. They may exist either as steady-state currents or as pulses of

current carried by Alfvén waves. These FACs self-consistently alter the magnetospheric magnetic field until a new equilibrium is reached. In the terrestrial case, the scale for changes in these currents systems is quite brief, tens of seconds to a few minutes, because the Alfvén speed, V_A , is very high; i.e., of order 10^3 km/s everywhere outside of the plasma sheet. Based upon the M10 plasma and magnetic field results, similar speeds might be expected within the high latitude Hermean magnetosphere. For example, based upon the MIII encounter measurements in the high latitude magnetosphere typical values of $B \sim 50$ nT and $n_p \sim 1$ cm $^{-3}$ would appear to be representative with an implied Alfvén speed of $V_A = B/\sqrt{4\pi n_p m_p} \sim 1000$ km/s. However, if heavy ions such as O^+ or Na^+ are the dominant ion species, then the Alfvén speed would be reduced and the “bounce times” increased as much as a factor of ~ 6 . Still, as pointed out by Glassmeier (1997) and Luhmann et al. (1998), the transit time from a NMNL at $X \sim -3R_M$ to the surface of the planet at the lower latitude edge of the polar cap would be only ~ 10 s and the multiple reflections to reach equilibrium would take only ~ 1 min.

Three principal FAC systems are commonly observed at the Earth. The “Region 1” currents are driven by the solar wind interaction with the geomagnetic field at the magnetopause and its boundary layers. The “Region 2” currents are driven by plasma pressure gradients in the inner magnetosphere. And, third, the “substorm current wedge” currents in the midnight local time sector are generated by the pressure gradients generated in the near-tail by the braking of earthward directed high-speed flows out of the NENL. The sense of both the Region 1 and SCW systems is downward toward the planet on the dawn-side and outward on the dusk-side. Fig. 11 depicts the locations of these current systems at Mercury assuming that they are able to close near the surface by some as yet unknown mechanism. The Region 2 currents are not shown because the pressure gradients that drive them map to below the surface of Mercury according to the familiar 8 to 1 spatial scaling relation. Finally, Fig. 11 displays a portion of the induction currents that may be driven in the planetary interior by solar wind pressure variations (Glassmeier, 2000; Suess and Goldstein, 1979). The sense of these induction currents is to oppose rapid changes in the pre-existing magnetic field configuration so that the stress to which the B-field is responding is opposed.

In the early-1970s, it was thought that both Mercury and Mars might possess small intrinsic field magnetospheres. Although Mars Global Surveyor measurements (Acuna et al., 1998) have now shown that this is not the case for Mars, the possibility of twin small magnetospheres, one with no ionosphere (Mercury) and one with an ionosphere (Mars) more highly conducting than that of the Earth, spawned new ideas regarding the role of electrical conductance of the region at the foot of

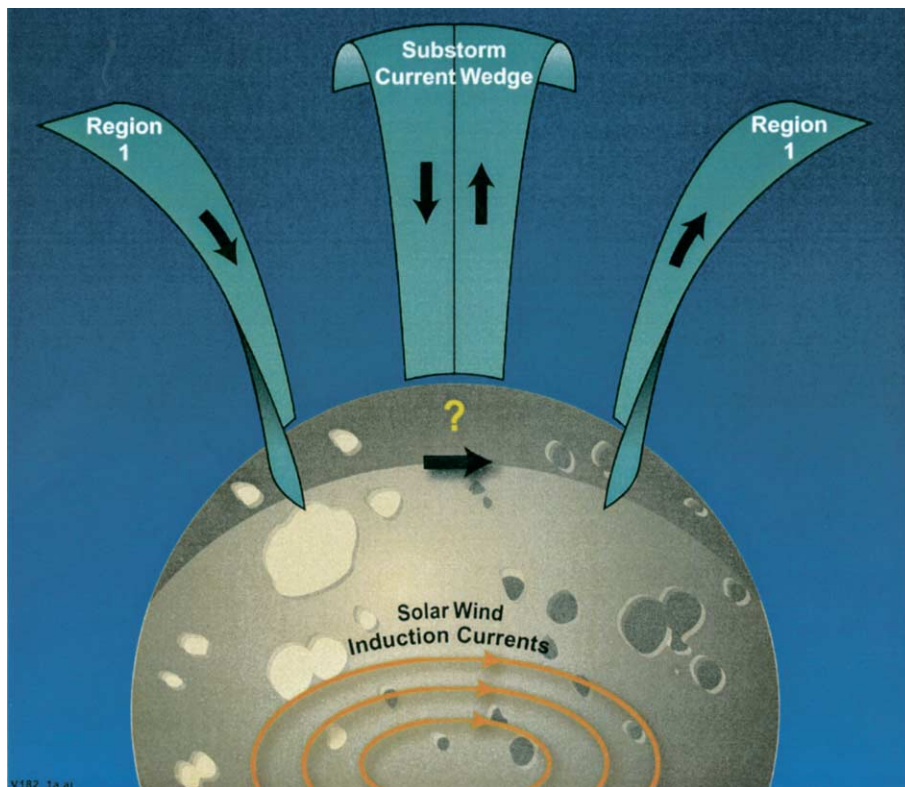


Fig. 11. Schematic view of the electrodynamic interaction between the magnetosphere and Mercury mediated by field aligned currents (green) and induction currents (orange).

magnetospheric flux tubes. Coroniti and Kennel (1973) argued that ionospheric conductivity will act as a “brake” or “regulator” on the rate of convection within magnetospheres. This effect, usually referred to as “line-tying”, occurs because ionospheric plasma, convecting in response to the electric field imposed by the magnetosphere, experiences a net drag force as a result of collisions with atmospheric neutral species. These collisions allow ionospheric ions and electrons some motion parallel to the direction of the electric field, as opposed to the $\mathbf{E} \times \mathbf{B}$ drift direction. In doing, they so generate Pederson conductivity that enables Joule dissipation. The greater the ionospheric Pederson conductivity is the larger the power that must be drawn from the solar wind to maintain a given electric potential across the polar cap. The lower the electrical conductivity in the polar cap is the closer the potential drop across the magnetosphere will approach to the maximum voltage applied by the solar wind, Φ_{SW} . Such effects have now been reproduced by global simulations (see Fedder and Lyon, 1987).

The electric potential applied to the magnetosphere is the product of the solar wind flow speed in the magnetosheath times the normal magnetic field component to the magnetopause integrated about the circumference of the tail lobes. However, it can be approximated by the product of the upstream solar wind speed, the compo-

nent of the IMF opposite to the planetary magnetic field at the dayside magnetopause and the length of the x-line at the dayside magnetopause (assumed to be comparable to the solar wind stand-off distance). Hence, given typical solar wind parameters at 1 AU, e.g., 400 km/s with an embedded southward IMF of magnitude 3 nT and a $10R_E$ width for the dayside x-line, the external Φ_{SW} applied to the Earth’s magnetosphere would be 77 kV. However, it should be noted during an encounter with a magnetic cloud embedded in a coronal mass ejection the Earth’s magnetosphere might experience a 500 km/s solar wind with southward IMF of 10 nT which corresponds to an applied electric potential of 320 kV. For Mercury at perihelion, the mean IMF intensity should be about a factor of 9 greater than that experienced at the Earth due to the $1/r^2$ gradient with distance from the sun. Accordingly, at Mercury perihelion typical solar wind conditions of 400 km/s and a southward IMF of -27 nT and an assumed day-side x-line width of $\sim 1.5R_M$ will result in the application of an electric potential of ~ 40 kV to the Hermean magnetosphere. For more extreme conditions corresponding to 500 km/s and -90 nT, the potential drop applied to the magnetosphere could reach 165 kV.

Rassbach et al. (1974) and Hill et al. (1976) built upon these concepts and further proposed that ionospheric conductivity may in turn affect the cross polar

cap potential, Φ_{pc} , by limiting the rate at which reconnection opens field lines at the dayside magnetopause. They argued that if ionospheric conductivity becomes high enough for the electric current closing across the planetary polar cap to generate significant magnetic fields at the magnetopause, then the reconnection process could be disrupted. In this manner Rassbach and Hill argued that ionospheric Pedersen conductance, Σ , limits the cross polar cap electric potential drop according to the relationship $\Phi_{pc} \leq \Phi_{sw}/(1 + \Sigma/\Sigma_0)$ where $\Sigma_0 \sim 20$ mho. At the Earth, the nightside ionosphere has a conductance of only a few mhos away from auroral arcs, but the dayside conductance can exceed 10 mho. Hence, the cross polar cap potential tends to “saturate” as it approaches $\Phi_{pc} = 2/3(\Phi_{sw})$. For this reason values over ~ 150 – 200 kV are seldom observed regardless of the potential applied by the solar wind (see Siscoe et al., 2002).

Based upon the available atmospheric models (Hunten et al., 1988), the height integrated conductance of Mercury’s nearly collisionless ionosphere has been estimated to be only $\sim 5 \times 10^{-6}$ mho (Lammer and Bauer, 1997). Surface conductance is a strong function of composition and mineralogy, but the value of 0.1 mho suggested by Hill et al. (1976) is not unreasonable. Alternative scenarios for generating electrical conductance, such as the pickup of newly created exospheric ions (Cheng et al., 1987) or photoelectron sheaths (Grard and Balogh, 2001; Grard et al., 1999) have not identified mechanisms for producing height integrated conductances greater than ~ 1 mho. Under these conditions, the electric potential drop across Mercury’s polar cap and magnetosphere should be set by the solar wind with $\Phi_{pc} \sim \Phi_{sw}$. Hence, at perihelion the typical electric potential drop across this small magnetosphere will typically reach a few tens of kilovolts with the average value at aphelion being less by a factor of ~ 2 .

Another expectation based upon the anticipated poor electrical conductivity of Mercury’s tenuous ionosphere and regolith is that the field aligned currents linking the magnetosphere and ionosphere may dissipate very rapidly as they quickly give up their energy to Joule heating in the highly resistive regolith. For these reasons, the strong variations in the east-west component of the magnetospheric magnetic field, B_y , measured by M10 between 20:50:55 to 20:51:18 during the first encounter, and displayed in Fig. 12 (from Slavin et al., 1997), came as a surprise. This bipolar variation in the $\Delta B_y \sim 60$ nT, was the largest perturbation in this component of the field recorded during either MI or MIII (also see Figs. 3 and 11). This magnetic signature is well known from measurements made by spacecraft traversing field-aligned current sheets in the Earth’s magnetosphere (Iijima and Potemra, 1978). At the time of the M10 FAC encounter it was located at $(-0.95R_M, -1.56R_M, 0.23R_M)$. The corresponding distance from the center of

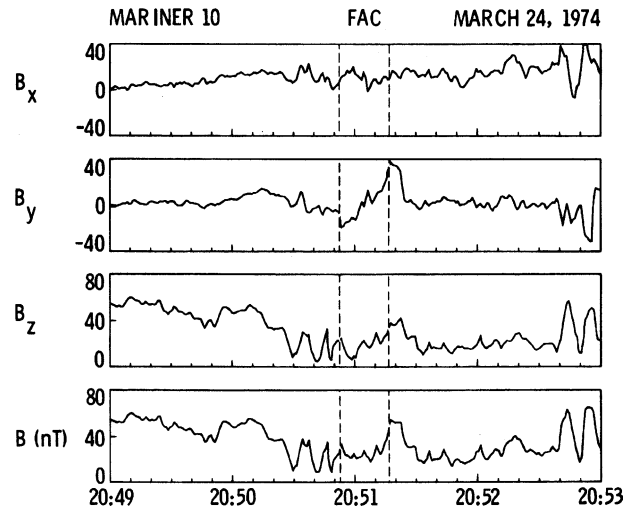


Fig. 12. Four minutes of M10 magnetic field measurements centered on the field-aligned current event identified.

the planet was $1.84R_M$ and the local time $\sim 03:50$. The average B_z around this event was about twice the magnitude of B_x as would be expected for a pass through the near-tail of the Earth at distance approaching geosynchronous orbit. Given the M10 trajectory (see Fig. 1), the gradient in B_y between the dashed lines is consistent with an upward FAC at the spacecraft. This upward current sheet is largely balanced by two smaller downward current sheets just before and after the central current sheet. Indeed, multiple current sheets are very common on the nightside of the auroral oval during substorms (Iijima and Potemra, 1978).

Given the strong central current sheet directed into the planet’s northern auroral zone at a point well east of midnight, Slavin et al. (1997) suggested the M10 FACs might be associated with the Region 1 currents which flow into the poleward edge of the auroral zone in the dawn hemisphere. Alternatively, it was also thought that they might be the eastern leg of the substorm current wedge that produced the magnetic field dipolarization encountered earlier around 20:48 (McPherron et al., 1973). This latter interpretation is of interest because of the substorm energetic particle injection observed a couple of minutes earlier. Under the assumption that the observed magnetic field perturbation is caused by a semi-infinite current sheet, the implied current density is ~ 50 mA/m. If this current sheet were indeed quasi-aligned with a constant L-shell, then the average current intensity in the central current sheet would be approximately $0.7 \mu\text{A}/\text{m}^2$. Both the sheet current intensity and current density inferred in this manner from the M10 observations lie within the range of values observed in the terrestrial magnetosphere (e.g., Iijima and Potemra, 1978). Although the current in the auroral oval at the Earth generally varies as a function of local time, solar wind, and substorm conditions, Slavin et al. estimated

the total current flowing into the auroral oval might be on this occasion to be 1.4×10^6 A. Again, this value lies within the $1\text{--}3 \times 10^6$ A range typically reported for the Region 1 currents at the Earth (Iijima and Potemra, 1978). However, these FAC observations must close and that raises the issue of the conductivity at low altitudes and the physical process(es) that support it.

The very short duration of the M10 substorm signatures, about 1–2 min, as compared with ~ 1 h at the Earth is also intertwined with the electrodynamics of the solar wind–magnetosphere–regolith system. Siscoe et al. (1975) argued that substorm duration is determined by the time necessary for plasma to convect across the polar cap or, equivalently, from the outer boundary of the tail down to the mid-plane where reconnection can take place. Using typical solar wind and magnetotail parameters, they showed that the ~ 1 h time scale for the terrestrial magnetosphere could be recovered. For Mercury the small dimensions of the magnetosphere and the intense inter-planetary $-V \times B$ electric fields in the inner heliosphere result in a much shorter rapid magnetic flux cycle time than that found in the tail of the Earth. The value calculated by Siscoe et al. was approximately 1 min, in good agreement with the duration of the energetic particle events.

Given these short time scales for magnetic flux cycling and the lack of terrestrial-style ionospheric line tying, Luhmann et al. (1998) suggested that substorms at Mercury may be largely “driven” by the solar wind. The terrestrial magnetosphere often stores magnetic flux for some variable amount time in the tail lobes before the system becomes unstable and NENL formation takes place. However, at other times it appears that the magnetosphere dissipates the energy drawn from the solar wind in a fashion that follows the inferred dayside reconnection rate in linear manner, but with a fixed phase lag (e.g., see Bargatze et al., 1985). These latter substorms are classified as being of the “driven” as opposed to “triggered” or “spontaneous”. The determination of how substorms within these two magnetospheres differ is an important objective for future missions to Mercury.

Experience with other magnetospheres, especially Jupiter’s, has shown the important electrodynamic effects of mass loading from planetary atmospheres and natural satellites. In the case of Mercury, Ip (1987) has suggested that there may be a strong tendency for ions to be “re-circulated” between the regolith and magnetosphere due to the large volume occupied by the planet and the dominance of finite gyro-radius effects in a magnetosphere of such small physical dimensions. Fig. 13 (from Ip, 1987) shows how the effects of ion impact sputtering, aided by solar radiation pressure, will result in the injection and acceleration of newly created ions followed by further re-circulation, if they impact and are implanted in the surface. The effects of these

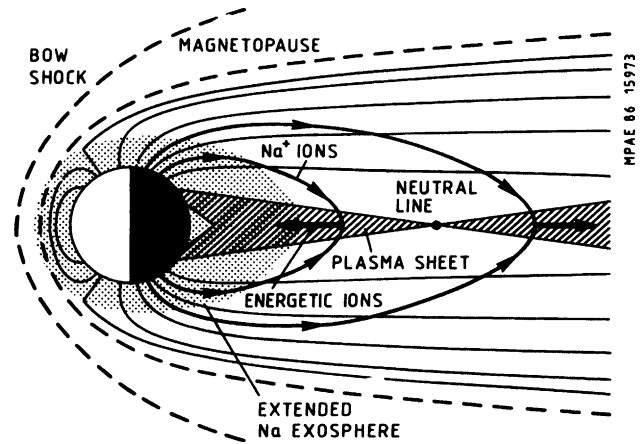


Fig. 13. Re-circulation of sodium sputtered from the surface, photo-ionized and carried back to the surface by magnetospheric convection.

heavy ions on Mercury’s magnetosphere are far from clear, but the pickup process itself is known to create a net electrical current that might contribute to FAC closure at low altitudes. Cheng et al. (1987) estimated that the magnitude of such a “pickup conductance” at Mercury could reach ~ 0.3 mho, but this number is highly uncertain. Similarly, Glassmeier (1997) calculated that the Alfvén conductance associated with MHD wave propagation could increase to ~ 1 mho if heavy ions were sufficiently plentiful. This is important because, as pointed out by Glassmeier, the SCW current system that appears to operate at Mercury based upon the M10 dipolarization and FAC observations would be very difficult to establish if the Alfvén conductance were too low. More detailed studies of ion pickup and acceleration are now being carried out in order to understand the similarities and differences between such processes at Mercury and the Earth (e.g., see Delcourt et al., 2002), but a definitive estimate of the effect of heavy ions on the electrodynamics of Mercury’s magnetosphere will require new measurements.

Killen et al. (2001, 2004) found that Mercury’s atmosphere is sufficiently tenuous that it would soon be depleted by losses associated with photo-ionization and charge exchange, if it were not being continuously replenished (see Goldstein et al., 1981). These sources and sinks are depicted in Fig. 14 (from Killen et al., 2001) where the state of Mercury’s atmosphere at any given moment corresponds to the integrated effect of all these mechanisms with significant change believed to occur on relatively short time scales of tens of hours to a few days. Consistent with the simulations of ion convection by Lukyanov et al. (2001), trajectory analyses conducted by Killen et al. (2004) indicate that perhaps 60% of these photo-ions may subsequently impact the surface, where they are adsorbed and become available for release via sputtering or impact vaporization. Furthermore, if reconnection at the dayside

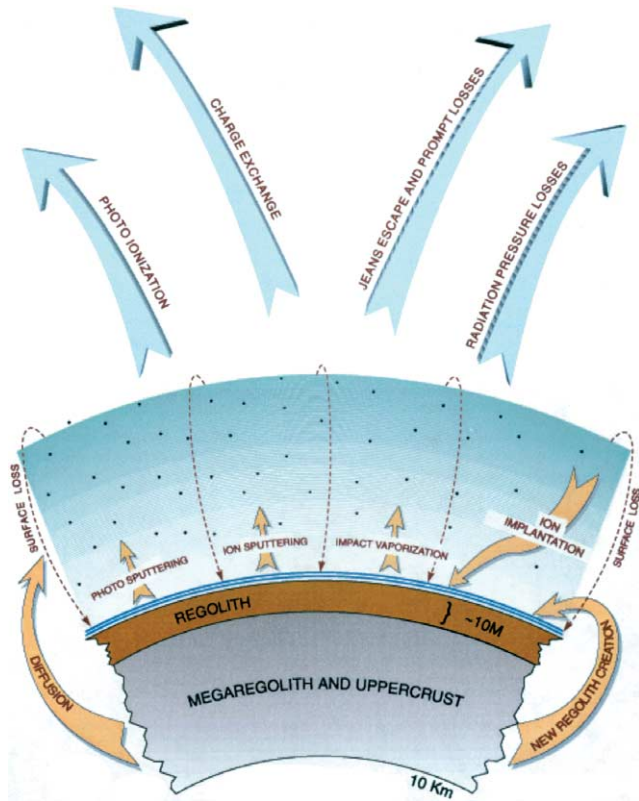


Fig. 14. Sources and sinks for Mercury's tenuous atmosphere. Reproduced by permission of the American Geophysical Union.

magnetopause frequently exposes significant fractions of the surface directly to impact by charged particles in the interplanetary medium, then the contribution of neutrals sputtered off by solar wind ions (Sarantos et al., 2001) and solar energetic particles (Leblanc et al., 2003) to the atmosphere may be a major driver for this system. In any event, the relatively short times required for photo-ionization, charge exchange and electron impact ionization will lead to sputtered neutrals being quickly ionized and picked-up by the convective flow within the magnetosphere producing a closely coupled system.

5. Summary

The Mariner 10 magnetic field measurements have shown that Mercury has a largely dipolar magnetic field tilted only slightly relative to the planetary spin axis. The interaction of this magnetic field with the solar wind creates a miniature magnetosphere that typically stands-off the solar wind at an altitude of $\sim 0.5R_M$ above the sub-solar point. Both MHD and hybrid numerical simulations of the solar wind interaction with Mercury support the terrestrial-type magnetosphere interpretation of the Mariner 10 observations. Hence, when combined with knowledge gained at the Earth and from

exploring the other planetary systems, it appears that the ~ 30 min of measurements taken by M10 were probably sufficient to determine the gross structure of this magnetosphere. However, it will not be until observations taken over an extended period of time, including perihelion passages, become available that the full range of structural variations can be known including its response to extreme solar wind conditions such as high speed streams and coronal mass ejections.

The internal dynamics of this miniature magnetosphere are, of course, more poorly understood. Estimates of the fraction of time that the magnetopause is sufficiently close to the planet to allow direct solar wind impact on the surface vary from a few per cent to several tens of per cent depending upon the assumed efficiency of magnetic reconnection and the strength of induction currents. The atmospheric neutral and magnetospheric charged particle populations may be closely coupled. A major source of neutrals is believed to be sputtering from the regolith due to solar wind ion, solar energetic particle and magnetospheric ion impact. And, in turn, the ionization of atmospheric neutrals is likely to be an important source of magnetospheric ions. The degree to which heavy ions of planetary origin, e.g., O^+ , Na^+ , K^+ , Mg^+ , etc., affect magnetospheric processes is a critical question that will be answered only with new measurements. Clear evidence of substorm activity was obtained during the second half of the first encounter in the form of an intense magnetic field dipolarization event and several energetic particle injections in the near-tail. To the extent that ion energy exceeds ~ 50 keV, they will generally be lost to surface impact or exit through the dayside magnetopause on time scales of 1–10 s. For this reason Mercury's magnetosphere may be ideal for investigations of deep tail charged particle acceleration because essentially all particles above certain energy can be assumed to have undergone such acceleration within seconds of their detection. With its complement of a magnetometer, an energetic charged particle spectrometer, a plasma analyzer with composition capability, and a ultraviolet imager (Solomon et al., 2001), the MESSENGER Mission appears well-suited to studying the dynamics of the magnetosphere during substorms and the exchange of mass between the magnetosphere, atmosphere and regolith.

The other unique aspect of Mercury's magnetosphere is its electrodynamic coupling to the solar wind above and the planet below. The brief, several minute duration of the substorm-like events observed by Mariner 10 has generally been attributed to the absence of an electrically conducting ionosphere and the resultant lack of line tying effects. Under these conditions it might be expected that the field-aligned currents driven by internal and external MHD stresses would be short lived and, therefore, rarely seen in spacecraft observations. It was therefore surprising, and perhaps very fortuitous, that

Mariner 10 observed both a magnetic dipolarization event and intense field-aligned currents during the outbound MI encounter. Detailed electric and magnetic field measurements of FACs at Mercury, whether carried by Alfvén waves or steady-state currents closing somehow at low altitudes, will be critical to achieving a full understanding of how this planet interacts with its magnetosphere. Despite the small dimensions of Mercury's magnetosphere, the strong interplanetary magnetic fields in the inner heliosphere and its lack of a conductive ionosphere should result in electric potential drops of some 10's of kV. The rapid convection driven by these relatively large dawn-to-dusk electric fields and the small dimensions of Mercury's magnetosphere are consistent with very brief substorm time scales observed by Mariner 10. For these reasons, the BepiColombo Mission with a low altitude planetary mapper and a high altitude magnetospheric orbiter carrying rather comprehensive magnetic and electric fields and charged and neutral particle instrumentation are well equipped to reveal the electrodynamic aspects of this magnetospheric system (Grard and Balogh, 2001; Blomberg, 1997).

In closing, we list just a few of most important science questions relating to Mercury's magnetosphere:

6. Solar wind–magnetosphere interaction

- How does the rate of magnetopause reconnection at Mercury's orbit differ from that at the Earth? What is the effect on solar wind stand-off distance? On the rate of energy transfer to the magnetosphere?
- How and where does the solar wind enter the magnetosphere?
- What effect does the very small IMF Parker spiral angle at Mercury have on the solar wind interaction and the magnetosphere?
- How often and where does the solar wind impact the planet?

7. Magnetosphere–planetary coupling

- What is the electric potential drop across the magnetosphere?
- What is the role of FACs in magnetosphere–planetary coupling at Mercury? How do field-aligned currents close?
- What effect do planetary induction currents exert on the system?
- What contributions do thermalized planetary ions make to the magnetospheric populations? How do they affect magnetospheric dynamics?
- Where, when, and how does reconnection take place in the tail? How does it differ from that observed at the Earth?

- How are substorms at Mercury different from those at Earth?

8. Charged particle acceleration

- What are the sources of Mercury's energetic particle populations? Planetary ion pick-up? Betatron? X-line acceleration?
- What roles do finite gyro-radius effects play in charged particle acceleration, transport, and equilibrium populations? Wave-particle interactions and diffusion?
- How do charged particle injections at Mercury differ from those at Earth?

Acknowledgements

We thank all of the people who contributed to the great success for the Mariner 10 mission especially the Principal Investigators for the magnetic field (N. Ness), plasma (H. Bridge) and cosmic ray (J. Simpson) investigations. Conversations with J. Gjerloev and E. Tanskanen on magnetosphere-ionosphere coupling are also gratefully acknowledged as are the very helpful suggestions made by both referees.

References

- Acuna, M.H. et al. Magnetic field and plasma observations at Mars: initial results from the Mars Global Surveyor mission. *Science* 279, 1676–1680, 1998.
- Angelopoulos, V., Baumjohann, W., Kennel, C.F., et al. Bursty bulk flows in the inner central plasma sheet. *J. Geophys. Res.* 97, 4027–4039, 1992.
- Baker, D.N., Simpson, J.A., Eraker, J.H. A model of impulsive acceleration and transport of energetic particles in Mercury's magnetosphere. *J. Geophys. Res.* 91, 8742–8748, 1986.
- Baker, D.N., Pulkkinen, T.I., Angelopoulos, V., Baumjohann, W., McPherron, R.L. Neutral line model of substorms: past results and present view. *J. Geophys. Res.* 101, 12975–13010, 1996.
- Bargatze, L.F., Baker, D.N., McPherron, R.L., Hones Jr., E.W. Magnetospheric impulse response for many levels of geomagnetic activity. *J. Geophys. Res.* 90, 6387–6394, 1985.
- Baumjohann, W., Paschmann, G., Luhr, H. Characteristics of high speed ion flows in the plasma sheet. *J. Geophys. Res.* 95, 3801–3809, 1990.
- Blomberg, L.G. Mercury's magnetosphere, exosphere and surface: low-frequency field and wave measurements as a diagnostic tool. *Planet. Space Sci.* 45, 143–148, 1997.
- Cheng, A.F., Johnson, R.E., Krimigis, S.M., Lanzerotti, L.J. Magnetosphere, exosphere and surface of Mercury. *Icarus* 71, 430–440, 1987.
- Christon, S.P. A comparison of the Mercury and Earth magnetospheres: electron measurements and substorm time scales. *Icarus* 71, 448–471, 1987.
- Connerney, J.E.P., Ness, N.F. The magnetosphere of Mercury, in: Chapman, C. (Ed.), *Mercury*. University of Arizona Press, pp. 494–513, 1988.

- Coroniti, F.V., Kennel, C.F. Can the ionosphere regulate magnetospheric convection? *J. Geophys. Res.* 78, 2837–2851, 1973.
- Cowley, S.W.H. Plasma populations in a simple open model magnetosphere. *Space Sci. Rev.* 25, 217–275, 1980.
- Delcourt, D.C., Moore, T.E., Orsini, S., Millilo, A., Sauvaud, J.-A. Centrifugal acceleration of ions near Mercury. *Geophys. Res. Lett.* 29 (12), 2002, doi:10.1029/2001GL013829.
- Eraker, J.H., Simpson, J.A. Acceleration of charged particles in Mercury's magnetosphere. *J. Geophys. Res.* 91, 9973–9993, 1986.
- Fedder, J.A., Lyon, J.G. The solar wind–magnetosphere–ionosphere current–voltage relationship. *Geophys. Res. Lett.* 14, 880–883, 1987.
- Giampieri, G., Balogh, A. Modeling of magnetic field measurements at Mercury. *Planet. Space Sci.* 49, 1637–1642, 2001.
- Glassmeier, K.-H. The Hermean magnetosphere and its I–M coupling. *Planet. Space Sci.* 45, 119–125, 1997.
- Glassmeier, K.-H. Currents in Mercury's Magnetosphere, Magnetospheric Current Systems. AGU, Washington, DC, 2000, pp. 371–380.
- Goldstein, B.E., Suess, S.T., Walker, R.J. Mercury: magnetospheric processes and the atmospheric supply and loss rates. *J. Geophys. Res.* 86, 5485–5499, 1981.
- Grard, R., Balogh, A. Return to Mercury: science and mission objectives. *Planet. Space Sci.* 49, 1395–1407, 2001.
- Grard, R., Laakso, H., Pulkkinen, T.I. The role of photoemission in the coupling of the Mercury surface and magnetosphere. *Planet. Space Sci.* 47, 1459–1463, 1999.
- Hill, T.W., Dessler, A.J., Wolf, R.A. Mercury and Mars: the role of ionospheric conductivity in the acceleration of magnetospheric particles. *Geophys. Res. Lett.* 3, 429–432, 1976.
- Hood, L.L., Schubert, G. Inhibition of solar wind impingement on Mercury by planetary induction currents. *J. Geophys. Res.* 84, 2641–2647, 1979.
- Hunten, D.M., Morgan, T.H., Schemansky, D.E. The Mercury atmosphere, in: Chapman, C. (Ed.), *Mercury*. University of Arizona Press, Tucson, pp. 562–612, 1988.
- Ieda, A., Machida, S., Mukai, T., Saito, Y., Yamamoto, T., Nishida, A., Terasawa, T., Kokubun, S. Statistical: analysis of plasmoid evolution with GEOTAI observations. *J. Geophys. Res.* 103, 4453–4465, 1998.
- Iijima, T., Potemra, T.A. Large-scale characteristics of field-aligned currents associated with substorms. *J. Geophys. Res.* 83, 599–615, 1978.
- Ip, W.-H. Dynamics of electrons and heavy ions in Mercury's magnetosphere. *Icarus* 71, 441–447, 1987.
- Ip, W.-H., Kopp, A. MHD simulation of the solar wind interaction with Mercury. *J. Geophys. Res.* 107 (A11), 1348, 2002, doi:10.1029/2001JA009171.
- Kabin, K., Gombosi, T.I., et al. Interaction of Mercury with the solar wind. *Icarus* 84, 397–406, 2000.
- Kallio, E., Janhunen, J.P. Modeling the solar wind interaction with Mercury by a quasi-neutral hybrid model. *Ann. Geophys.* 21 (11), 2133–2145, 2003.
- Killen, R.M., Potter, A.E., Reiff, P., et al. Evidence for space weather at Mercury. *J. Geophys. Res.* 106, 20509–20525, 2001.
- Killen, R.M., Sarantos, M., Reiff, P. Space weather at Mercury. *Adv. Space Res.*, 2004 (doi:10.1016/j.asr.2003.02.020).
- Korth, H., Anderson, B.J., McNutt, R.L., Jr., et al., Determination of the properties of Mercury's magnetic field by the MESSENGER mission. *Planet. Space Sci.*, 2004 (in press).
- Lammer, H., Bauer, S.J. Mercury's exosphere: origin of surface sputtering and implications. *Planet. Space Sci.* 45, 73–79, 1997.
- Leblanc, F., Luhmann, J.G., Johnson, R.E., Lui, M. Solar energetic particle event at Mercury. *Planet. Space Sci.* 51, 339–352, 2003.
- Luhmann, J.G., Russell, C.T., Tsyganenko, N.A. Disturbances in Mercury's magnetosphere: are the Mariner 10 “substorms” simply driven. *J. Geophys. Res.* 103, 9113–9119, 1998.
- Lukyanov, A.V., Barabash, S., Lundin, R., son Brandt, P.C. Energetic neutral atom imaging of Mercury's magnetosphere: 2. Distribution of energetic charged particles in a compact magnetosphere. *Planet. Space Sci.* 49, 1677–1684, 2001.
- McPherron, R.L., Russell, C.T., Aubry, M.P. Satellite studies of magnetospheric substorms on August 15, 1968, 9. Phenomenological model for substorms. *J. Geophys. Res.* 78, 3131–3149, 1973.
- Ness, N.F., Behannon, K.W., Lepping, R.P., et al. Observations of magnetic field near Mercury: preliminary results from Mariner 10. *Science* 185, 151–159, 1974.
- Ness, N.F., Behannon, K.W., et al. Magnetic field of Mercury. *J. Geophys. Res.* 80, 2708–2716, 1975.
- Ness, N.F., Behannon, K.W., et al. Observations of Mercury's magnetic field. *Icarus* 28, 479–488, 1976.
- Ogilvie, K.W., Scudder, J.D., Hartle, R.E., et al. Observations at Mercury encounter by the plasma science instrument on Mariner 10. *Science* 185, 145–150, 1974.
- Ogilvie, K.W., Scudder, J.D., Vasyliunas, V.M., Hartle, R.E., Siscoe, G.L. Observations at the planet Mercury by the plasma electron instrument: Mariner 10. *J. Geophys. Res.* 82, 1807–1824, 1977.
- Potter, A.E., Morgan, T.H. Discovery of sodium in the atmosphere of Mercury. *Science* 229, 651–653, 1985.
- Potter, A.E., Morgan, T.H. Potassium in the atmosphere of Mercury. *Icarus* 67, 336–340, 1986.
- Potter, A.E., Killen, R.M., Morgan, T.H. Rapid changes in the atmosphere of Mercury. *Planet. Space Sci.* 47, 1441–1448, 1999.
- Rassbach, M.E., Wolf, R.A., Daniell Jr., R.E. Convection in a Martian magnetosphere. *J. Geophys. Res.* 79, 1125–1127, 1974.
- Richardson, I.G., Cowley, S.W.H., Hones Jr., E.W., Bame, S.J. Plasmoid-associated energetic ion bursts in the deep geomagnetic tail: properties of plasmoids and the post-plasmoid plasma sheet. *J. Geophys. Res.* 92, 9997–10013, 1987.
- Richardson, I.G., Owen, C.J., Slavin, J.A. Energetic (>0.2 MeV) electron bursts in the deep geomagnetic tail observed by the Goddard space flight center experiment on ISEE-3: association with geomagnetic substorms. *J. Geophys. Res.* 101, 2723–2740, 1996.
- Russell, C.T. On the relative locations of the bow shocks of the terrestrial planets. *Geophys. Res. Lett.* 4, 387–390, 1977.
- Russell, C.T., Walker, R.J. Flux transfer events at Mercury. *J. Geophys. Res.* 90, 11067–11074, 1985.
- Russell, C.T., Baker, D.N., Slavin, J.A. The magnetosphere of Mercury, in: Chapman, C. (Ed.), *Mercury*. University of Arizona Press, Tucson, pp. 514–561, 1988.
- Russell, C.T. ULF waves in the Mercury magnetosphere. *Geophys. Res. Lett.* 16, 1253–1256, 1989.
- Sarantos, M., Reiff, P.H., Hill, T.W., Killen, R.M., Urquhart, A.L. A B_x -interconnected magnetosphere model for Mercury. *Planet. Space Sci.* 49, 1629–1635, 2001.
- Sarris, E.T., Axford, W.I. Energetic protons near the plasma sheet boundary. *Nature* 77, 460–462, 1979.
- Shiokawa, K., Baumjohann, W., Haerendel, G., et al. High-speed ion flow, substorm current wedge formation and multiple Pi2 pulsations. *J. Geophys. Res.* 103, 4491–4507, 1998.
- Sibeck, D.G., Lopez, R.E., Roelof, B.C. Solar wind control of magnetopause shape, location and motion. *J. Geophys. Res.* 96, 5489–5495, 1991.
- Simpson, J.A., Eraker, J.H., Lamport, J.E., Walpole, P.H. Electrons and protons accelerated in Mercury's magnetosphere. *Science* 185, 160–166, 1974.
- Siscoe, G.L., Christopher, L. Variations in the solar wind stand-off distance at Mercury. *Geophys. Res. Lett.* 2, 158–160, 1975.
- Siscoe, G.L., Ness, N.F., Yeates, C.M. Substorms on Mercury? *J. Geophys. Res.* 80, 4359–4363, 1975.

- Siscoe, G.L. et al. Hill model of transpolar potential saturation: comparisons with MHD models. *J. Geophys. Res.* 107 (A6), 2002, doi: [10.1029/2001JA000109](https://doi.org/10.1029/2001JA000109).
- Slavin, J.A., Holzer, R.E. The effect of erosion on the solar wind stand-off distance at Mercury. *J. Geophys. Res.* 84, 2076–2082, 1979.
- Slavin, J.A., Holzer, R.E. Solar wind flow about the terrestrial planets, 1. Modeling bow shock position and shape. *J. Geophys. Res.* 86, 11401–11418, 1981.
- Slavin, J.A., Owen, C.J., J.Connerney, E.P., Christon, S.P. Mariner 10 observations of field-aligned currents at Mercury. *Planet. Space Sci.* 45, 133–141, 1997.
- Slavin, J.A. et al. Dual spacecraft observations of lobe magnetic field perturbations before, during and after plasmoid release. *Geophys. Res. Lett.* 26, 2897–2900, 1999.
- Slavin, J.A., Fairfield, D.H., Lepping, R.P., et al. Simultaneous observations of earthward flow bursts and plasmoid ejection during magnetospheric substorms. *J. Geophys. Res.* 107 (A7), 2002, doi:[10.1029/2000JA003501](https://doi.org/10.1029/2000JA003501).
- Solomon, S.C. et al. The MESSENGER mission to Mercury, scientific objectives and implementation. *Planet. Space Sci.* 49, 1445–1465, 2001.
- Suess, S.T., Goldstein, B.E. Compression of the Hermaean magnetosphere by the solar wind. *J. Geophys. Res.* 84, 3306–3312, 1979.